Structural Mechanism of the Phase Transitions in the Mg−Cu−Mo_6S_8 System Probed by ex Situ Synchrotron X-ray Diffraction

E. Levi,*,† A. Mitelman,† D. Aurbach,† and M. Brunelli‡

Department of Chemistry, Bar-Ilan University, Ramat-Gan, Israel 52900, and ESRF, 6 rue Jules Horowitz, BP 220, F-38043 Grenoble Cedex, France

Received June 10, 2007. Revised Manuscript Received July 18, 2007

Mo_6S_8 is a unique cathode material for rechargeable magnesium batteries, but its theoretical capacity cannot be realized at ambient temperature due to partial Mg trapping. This work shows that this trapping can be avoided by using $Cu_{\sim 1}Mo_6S_8$ instead of Mo_6S_8. The phase diagram of Mg insertion into $Cu_{\sim 1}$-Mo_6S_8 was studied by a combination of cyclic voltammetry and ex situ synchrotron X-ray diffraction. Similarly to the previously studied Li−M−Mo_6S_8 (M = metal) systems, the insertion results in Cu extrusion from the intercalation compound, but contrary to the known cases, this process is fully reversible. The structural mechanism of the insertion reactions was established by Rietveld analysis performed for nine new $Mg_xCu_yMo_6S_8$ phases. It was found that the crystal structure of the quaternary intercalation compounds in the Mg−Cu−Mo_6S_8 system is similar to that of the ternary phases: both Mg^{2+} and Cu^+ cations are located in the tetrahedral sites of the inner and outer rings, while the occupancy of the sites increases with intercalation level. However, the cation distribution is not disordered. It can be characterized by (i) Mg preference for the inner sites and (ii) cation segregation. The latter is typical for the separate cation groups in the same intercalation compound, but it appears also as cation segregation in different phases. As a result, similarly to the previously studied Li−Cu−Mo_6S_8 system, the phase diagram of Mg insertion into $Cu_{\sim 1}Mo_6S_8$ is rather complex. It includes three phase regions and the coexistence of Cu-rich and Cu-depleted compounds. The structural mechanism proposed in this work sheds light on the electrochemical behavior of the $Cu_{\sim 1}Mo_6S_8$ electrodes in Mg battery; in particular, it explains the absence of Mg trapping.

Introduction

Chevrel phases (CPs), $M_xMo_6T_8$ (M = metal, T = S, Se), were intensively studied in the past because of their remarkable electromagnetic, thermoelectric, and catalytic properties.[1−4] In addition, the unusual crystal structure, namely, the presence of the Mo_6 clusters that can easily adopt up to four electrons,[1,2] ensures an exceptionally high mobility of multivalent cations in the Mo_6T_8 hosts.[5] As a result, the latter are suggested as unique cathode materials in rechargeable Mg batteries.[6,7] The battery functionality is based on the reversible insertion/extraction reactions,[8] which can be classified as classic phase transitions:

$$Mg^{2+} + 2e^- + Mo_6T_8 \leftrightarrow MgMo_6T_8 \quad \text{(stoichiometric compound)} \quad (1)$$

$$Mg^{2+} + 2e^- + MgMo_6T_8 \leftrightarrow Mg_2Mo_6T_8 \quad \text{(stoichiometric compound)} \quad (2)$$

The theoretical capacity for Mo_6S_8 (122 mA·h/g) is essentially higher than that for Mo_6Se_8 (83 mA·h/g). However, whereas the electrochemical behavior of the selenide host is fully reversible, Mg trapping occurs in the sulfide (Figure 1), i.e., about 25% of Mg can be extracted from the $Mg_xMo_6S_8$ ($0 < x < 2$) electrodes only at elevated temperature.[8,9] It was shown that this trapping is caused by a unique ring arrangement of closely located cation sites with low potential energy.[10,11] It exists only for $x < 1$, i.e., upon removal of the last inserted cation per formula unit. The extraction of Mg from $Mg_xMo_6S_8$ for $x > 1$ is fast because the repulsion between two Mg^{2+} cations per formula unit promotes their transport throughout the material bulk. Thus, it can be suggested that trapping may be avoided by excluding the problematic stage of the full cation removal

* To whom correspondence should be addressed.
† Bar-Ilan University.
‡ ESRF.

(1) Yvon, K. In *Current Topics in Material Science*; Kaldis, E., Ed.; Elsevier: North-Holland, Amsterdam, 1979; Vol. 3.
(2) *Topics in Current Physics: Superconductivity in Ternary Compounds I*; Fisher, Ø., Maple, M. B., Eds.; Springer-Verlag: Berlin, 1982.
(3) Nunes, R. W.; Mazin, I. I.; Sigh, D. *J. Phys. Rev. B* **1999**, *59*, 7969.
(4) Benson, J. W.; Schrader, G. L.; Angelici, R. J. *J. Mol. Catal. A: Chem.* **1995**, *96*, 283.
(5) Schollhorn, R. *Angew. Chem., Int. Ed. Engl.* **1980**, *19*, 983.
(6) Aurbach, D.; Lu, Z.; Schechter, A.; Gofer, Y.; Gizbar, H.; Turgeman, R.; Cohen, Y.; Moskovich, M.; Levi, E. *Nature* **2000**, *407*, 724.
(7) Aurbach, D.; Weissman, I.; Gofer, Y.; Levi, E. *Chem. Record* **2003**, *3*, 61.
(8) Levi, M. D.; Lancry, E.; Levi, E.; Gizbar, H.; Gofer, Y.; Aurbach, D. *Solid-State Ionics* **2005**, *176*, 1695.
(9) Lancry, E.; Levi, E.; Gofer, Y.; Levi, M.; Salitra, G.; Aurbach, D. *Chem. Mater.* **2004**, *16*, 2832.
(10) Levi, E.; Lancry, E.; Mitelman, A.; Aurbach, D.; Ceder, G.; Morgan, D.; Isnard, O. *Chem. Mater.* **2006**, *18*, 5492.
(11) Levi, E.; Lancry, E.; Mitelman, A.; Aurbach, D.; Isnard O.; Djurado D. *Chem. Mater.* **2006**, *18*, 3705.

10.1021/cm0715489 CCC: $37.00
Published on Web 09/19/2007

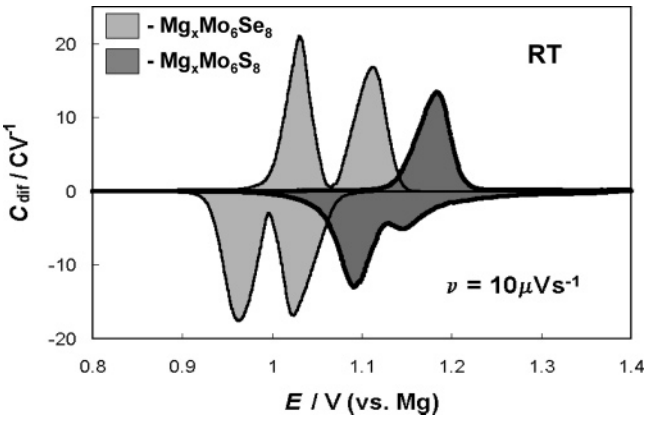

Figure 1. Slow scan cyclic voltammetry curves (plots of current I vs potential E, presented in the form of the differential capacitance, $C_{dif} = I/\nu$, where ν is the potential scan rate, equal to 10 μV/s) for Mg^{2+} ion insertion into Mo_6T_8 (T = S, Se). Redox peaks correspond to the phase transitions described in reactions (1) and (2).

from the sulfide, namely, by using metal-containing CPs host, $B_yMo_6S_8$, instead of pure Mo_6S_8.

The electrochemical cycling of $Mg_xB_yMo_6S_8$ electrodes should be based on the displacement reactions discovered previously for Li or Na insertion into different metal-containing CPs:[12−25]

$$4/nA^{n+} + B^{m+}{}_yMo_6T_8 + 4e^- \rightarrow A_{4/n}Mo_6T_8 + yB^0 \quad (3)$$

It was shown that the B metal extrusion from the CP structure occurs at the last insertion stages when the total cation charge exceeds four electrons per formula unit:

$$nx + my > 4 \quad (4)$$

(Here x is the amout of inserted cations A^{n+}). The formation of mixed quaternary compounds, $A^{n+}{}_xB^{m+}{}_yMo_6T_8$, upon the earlier stages (before metal extrusion) was reported,[12−17] but their crystal structure was not studied. Moreover, in the CP systems described in the literature,[12−25] the metal extraction was mostly irreversible: After a few cycles, the electrodes behaved as the binary hosts.

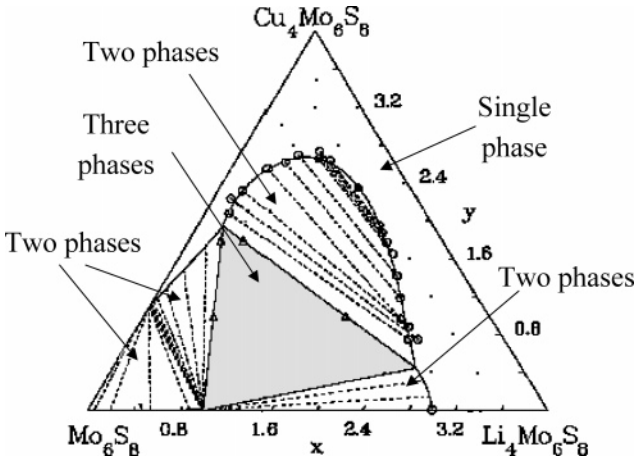

Figure 2. Phase diagram of the Li−Cu−Mo_6S_8 system with the tie lines (dashed lines) in the two-phase regions (according to ref 14).

However, for other metal-containing hosts such as copper vanadates[26−28] or intermetallic compounds,[29−31] it is known that the displacement reactions can be reversible. The latter case should be of practical interest for the Mg−$Cu_yMo_6S_8$ system because of the expected positive influence of the cations' repulsion on their mobility. In addition, the use of $Cu_yMo_6S_8$ instead of Mo_6S_8 avoids the leaching stage in the electrode preparation. Actually, in contrast to the metastable Mo_6S_8, $Cu_yMo_6S_8$ ($y \approx 2$) can be obtained directly by solid-state synthesis,[1,2] and even in practical amounts by the molten salt method,[32] while in the latter case after the salt dissolution y is commonly close to 1.

According to parallel electrochemical studies that will be published in a separate paper, the rate capability of the $Cu_{\sim 1}$-Mo_6S_8 cathodes in rechargeable Mg batteries is considerably higher than that of Mo_6S_8. Moreover, in contrast to the previous systems,[12−25] the cycling of the $Mg_xCu_yMo_6S_8$ cathodes is fully reversible. It can be suggested that the Cu metal, which has been removed from the CP crystal structure upon Mg intercalation into $CuMo_6S_8$, is reinserted upon Mg extraction, with no charge-trapping phenomena. However, it is clear that the knowledge of the phase diagram of Mg insertion into the $Cu_yMo_6S_8$ host is needed to understand the mechanism of the displacement reactions.

In spite of the variety of studied Li−$B_yMo_6T_8$ systems (B = Ag, Ni, Cu, In, Fe, and Co),[12−25] phase diagrams were established only for Li insertion into $Cu_yMo_6T_8$.[13−17] For T = S, the phase diagram is rather complex (Figure 2). A single phase, $Li_xCu_yMo_6S_8$, exists only for relatively high values of x and y. In many cases Li insertion results in a mixture of two, or even three, phases. Note that equilibrium of three

(12) Schollhorn, R. In *Inclusion Compounds*, v. 1; Atwood, J. L., Ed.; Academic Press: London, 1984.
(13) McKinnon, W. R.; Dahn, J. R. *Solid State Commun.* **1984**, *52*, 245.
(14) McKinnon, W. R.; Dahn, J. R.; Jui, C. C. H. *J. Phys. C: Solid State Phys.* **1985**, *18*, 4443.
(15) Jui, C. C. H.; McKinnon, W. R.; Dahn, J. R. *Phys. Rev. Lett.* **1985**, *54*, 1432.
(16) Selwyn, L. S.; McKinnon, W. R. *J. Phys. C: Solid State Phys.* **1988**, *21*, 1905.
(17) Selwyn, L. S.; McKinnon, W. R.; Le Page, Y. *Phys. Rev. B* **1990**, *42*, 10427.
(18) Takeda, Y.; Kanno, R.; Noda, M.; Yamamoto, O. *Mater. Res. Bull.* **1985**, *20*, 71.
(19) Tarascon, J. M.; Hull, G. W.; Marsh, P.; Ter Haar. *J. Solid State Chem.* **1987**, *66*, 204.
(20) Tarascon, J. M.; Orlando, T. P.; Neal, M. J. *J. Electrochem. Soc.* **1988**, *135*, 804.
(21) Wakihara, M.; Uchida, T.; Suzuki, K.; Taniguchi, M. *Electrochem. Acta* **1989**, *34*, 867.
(22) Uchida, T.; Tanjo, Y.; Wakihara, M.; Taniguchi, M. *J. Electrochem. Soc.* **1990**, *137*, 7.
(23) Yamaguchi, S.; Uchida, T.; Wakihara, M. *J. Electrochem. Soc.* **1991**, *138*, 687.
(24) Guohua, L.; Ikuta, H.; Uchida, T.; Wakihara, M. *J. Power Sources* **1995**, *54*, 519.
(25) Suzuki, K.; Iijima, T.; Wakihara, M. *Solid-State Ionics* **1998**, *109*, 311.
(26) Morcrette, M.; Rozier, P.; Dupont, L.; Mugnier, E.; Sannier, L.; Galy, J.; Tarascon, J.-M. *Nat. Mater.* **2003**, *2*, 755.
(27) Rozier, P.; Morcrette, M.; Martin, P.; Laffont, L.; Tarascon, J.-M. *Chem. Mater.* **2005**, *17*, 984.
(28) Morcrette, M.; Martin, P.; Rozier, P.; Vezin, H.; Chevallier, F.; Laffont, L.; Poizot, P.; Tarascon, J.-M. *Chem. Mater.* **2005**, *17*, 418.
(29) Thackeray, M. M.; Vaughey, J. T.; Kahaian, A. J.; Kepler, K. D.; Benedek, R. *Electrochem. Commun.* **1999**, *1*, 111.
(30) Fransson, L. M. L.; Vaughey, J. T.; Benedek, R.; Edstrom, K.; Thomas, J. O.; Thackeray, M. M. *Electrochem. Commun.* **2001**, *3*, 317.
(31) Fransson, L. M. L.; Vaughey, J. T.; Edstrom, K.; Thackeray, M. M. *J. Elecrochem. Soc.* **2003**, *150*, A86.
(32) Lancry, E.; Levi, E.; Mitelman, A.; Malovany, S.; Aurbach, D. *J. Solid State Chem.* **2006**, *179*, 1879.

coexisting phases is very unusual for intercalation reactions, but the most remarkable feature is the change in the composition of these phases.

First, in contrast to classic insertion reactions, in the Li−Cu−Mo_6S_8 system two coexisting compounds are commonly nonstoichiometric, and their composition changes continuously upon Li intercalation (In Figure 2 these phases are connected to each other by the tie lines). In addition, Cu_y-Mo_6S_8 cannot be regarded as the usual host with constant composition: For most of the regions in the phase diagram, Li insertion into $Cu_yMo_6S_8$ leads to cation segregation, i.e., the intercalation products are composed of coexisting Cu-rich and Cu-depleted phases. For instance, within the gray triangle in Figure 2, the material is a mixture of $LiMo_6S_8$, $Li_{2.5}Cu_{0.5}Mo_6S_8$, and almost pure $Cu_2Mo_6S_8$. This cation segregation indicates a high mobility not only for the inserted Li^+ cations but also for the Cu^+ ions as well. A similar complex behavior of two mobile cations can be expected for the Mg−Cu−Mo_6S_8 system, but any prediction of the insertion reactions cannot be done without knowledge of the crystal structure of the intercalation compounds.

According to the literature,[1,2,10,33] the crystal structures of Cu-, Li-, and Mg-containing CP sulfides are very similar: The cations are distributed on the tetrahedral sites in the cavities between the Mo_6S_8 blocks. The cation sites form so-called inner and outer rings (six sites per ring). Each ring can adopt up to one Mg[10] or two Cu atoms.[1,2] In the case of Li, the adaptation ability of the rings is different: only one cation can be located in the inner ring and three cations can be located in the outer ring.[33] A random distribution of the cations in the rings results in the rhombohedral symmetry of the crystals. The inner ring has a lower potential energy than the outer one.[10] Thereby, in these compounds the inner sites are occupied at the first stages of cation insertion.

Based on the structural similarity of these compounds and the close values of the average cation−sulfur bonds[34] (2.45, 2.44, and 2.37 Å for Li^+, Mg^{2+}, and Cu^+ cations, respectively), formation of substitutional Li−Cu or Mg−Cu solid solutions can be suggested. However, the complex phase diagram of the Li−Cu−Mo_6S_8 system mentioned above shows that such simple structural considerations are insufficient for understanding the insertion mechanism. Moreover, in spite of intensive studies of CPs in the past, the structural information for quaternary CPs is very poor. It seems that it exists only for $SnFe_xMo_6S_8$ ($0 \le x \le 0.4$), where the larger Sn^{2+} cations are located in the center of cavity 1, while the Fe^{2+} cations are distributed between the outer sites of cavity 2.[35]

Thus, the aim of this work was (i) to study the phase diagram of Mg insertion into a $Cu_yMo_6S_8$ ($1 \le y \le 2$) host, with the emphasis on the crystal structure of the mixed intercalation compounds, (ii) to explain the electrochemical behavior of $Cu_yMo_6S_8$ cathodes upon the reversible insertion of magnesium, and (iii) to clarify a general structural mechanism for the phase transitions in the CP systems with two mobile cations. The presence of two types of cations moving in opposite directions in the same intercalation material, $Mg_xCu_yMo_6S_8$, as well as the possible formation of solid solutions with an unusual Cu ⇔ Mg substitution, seems to be very attractive for general fundamental studies.

The best method for determining the cation position in the air-sensitive CPs is neutron diffraction.[10,11] However, as will be shown below, the process under study includes the formation of compounds with very close unit cell parameters. Thus, synchrotron X-ray high-resolution powder diffraction is needed to identify these compounds. It is clear that in situ diffraction measurements are preferable for following the changes in the phase composition upon intercalation processes. This approach was not adopted in this work due to the sensitivity of the relevant electrolyte solutions to atmospheric contaminants and the relatively long time needed for the complicated electrochemical experiments. However, in spite of the limitations of ex situ measurements, it was possible in this work to decipher the structural mechanism of Mg intercalation into the $Cu_{\sim 1}Mo_6S_8$ host, which sheds light on its unique electrochemical behavior.

Experimental Section

The materials under study were obtained in three different ways: (i) solid-state synthesis, (ii) chemical, and (iii) electrochemical intercalation. $Cu_{\sim 1}Mo_6S_8$ was prepared by a partial leaching of $Cu_{\sim 2}Mo_6S_8$. The leaching procedure and synthesis conditions for the first two methods were described previously.[9,10] The electrodes (80% active mass, 10% carbon black, and 10% PVdF binder pasted on stainless steel mesh, mass load ca. 10 mg/cm^2) were cycled in standard three-electrode cells (strips of Mg foil as counter and reference electrodes) at a current density of 0.1 mA/cm^2 using a VMP2 multichannel potentiostat (Princeton Applied Research) controlled by EC-Lab software or a 273A potentiostat/galvanostat (Princeton Applied Research) controlled by Corware software. The electrolyte solution was 0.25 M of $Mg(AlCl_2BuEt)_2$ in THF. The electrochemical processes were stopped at characteristic potentials. (See the points of the slow scan cyclic voltammetry curve in Figure 3.) The electrodes were then removed from the cell, washed by THF, and dried. The active mass was scratched out from the mesh and loaded into the glass capillaries for Synchrotron XRD measurements. All the preparations for the structural analysis were done in an Ar-containing glovebox.

Regular XRD measurements were performed with a Bruker Inc. (Germany) AXS D8 ADVANCE diffractometer (reflection $\theta-\theta$ geometry, Cu Kα radiation, receiving slit 0.2 mm, scintillation counter), equipped with a Gobel mirror (parallel beam). Diffraction data for Rietveld analysis were collected in the angular range of $10° < 2\theta < 110°$, step size 0.02°, step time 10 s/step. Synchrotron experiments were carried out in transmission mode at the high-resolution powder diffraction beamline ID31 of the European Synchrotron Radiation Facility (ESRF) in Grenoble, France. A wavelength of 0.35008(1) Å and 0.4-mm-diameter glass capillaries were used to prevent excessive material absorption. The fitting was done in the 2θ angular range from 1.8° to 35°.

The data were analyzed by the Rietveld structure refinement program, FULLPROF.[36] The Thompson-Cox-Hastings pseudo-Voigt function was used for the peak-shape approximation. The background was refined by a polynomial function (commonly four

(33) Ritter, C.; Gocke, E.; Fischer, C.; Schollhorn, R, J. *Mater. Res. Bull.* **1992**, *27*, 1217.
(34) Brese, N. E.; O'Keefee, M. *Acta Crystallogr.* **1991**, *B47*, 192.
(35) Vaishnava, P. P.; Kimball, C. W.; Matykiewicz, J. L.; Fradin, F. Y.; Shenoy, G. K.; Montano, P. A. *Phys. Rev. B* **1986**, *34*, 4599.
(36) Carjaval, J. R. *Physica B* **1993**, *192*, 55.

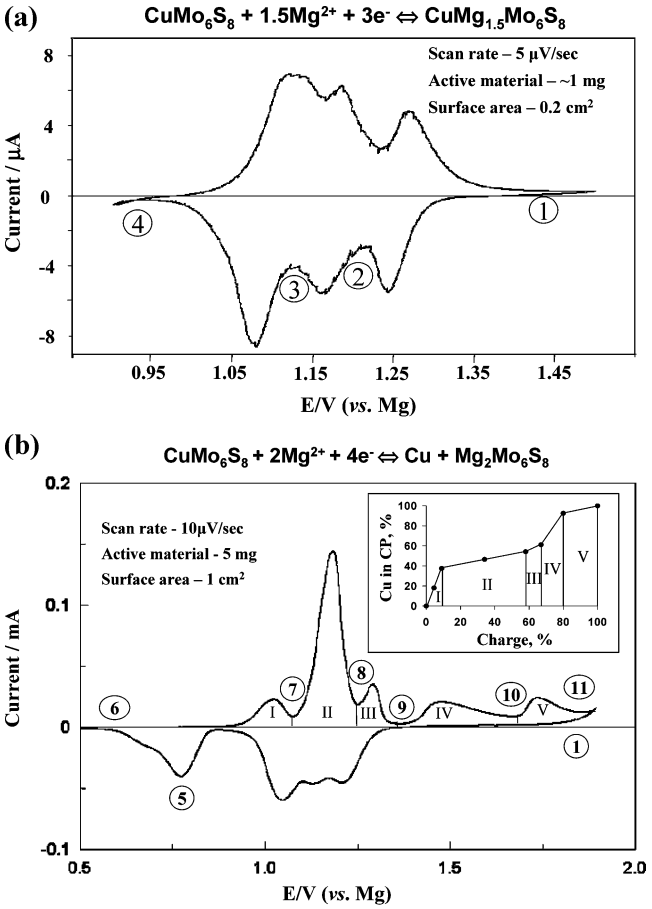

Figure 3. Slow scan cyclic voltammetry curves for Mg^{2+} ion insertion into $CuMo_6S_8$: (a) cycling between 1.5 and 0.9 V; (b) cycling between 1.8 and 0.5 V. The insert presents the change in the Cu amount in the CP materials upon electrode oxidation (the results of the electrochemical titration).

refined parameters). The atomic thermal parameters (0.33 Å^2 for Mo, 0.5 Å^2 for S, and 1 Å^2 for Mg and Cu) were chosen according to the literature data[2,37] and remained constant. Soft-distance constraints were applied to determine the cation positions in the structures. The agreement factors used in this article are defined according to the guidelines of the Rietveld refinement, which can be found elsewhere.[38] The validity of the refinements presented herein was verified by a comparison of the results with known ones. The atomic parameters for all the materials under study were very close to those of $Cu_{1.8}Mo_6S_8$ obtained by a single-crystal analysis[1,2] (see Supporting Information). The low *R*-factors obtained in the refinement, as well as reasonable values of the interatomic distances, cluster VECs, and bond valence sums for Cu^+ and Mg^{2+} cations, confirm the structural analysis presented in this paper.

Results and Discussion

Electrochemical Information. Detailed electrochemical studies of this system will be presented in separate papers. Below we present in brief some critical voltammetric features, according to which the structural analysis was carried out. Figures 3a and 3b present slow scan cyclic voltammetric (CV) curves for Mg insertion into $CuMo_6S_8$ electrodes. Each chart corresponds to a stabilized electrode (after four consecutive cycles). A comparison of these curves with those of the metal-free hosts (Figure 1) clarifies that the process of Mg insertion into $CuMo_6S_8$ is much more complicated and depends strongly on the potential range of cycling. To explain these features, it can be suggested first that Mg intercalation into $CuMo_6S_8$ is, in general, similar to that of Li insertion into metal-containing CPs (see reactions (3) and (4)).[12−25] In this case, the cycling in the short potential range between 1.5 and 0.9 V (Figure 3a) should be related to the Mg insertion into the host before Cu extrusion, while the last CV peak at low potential (about 0.8 V in Figure 3b) should be related to Cu extrusion and its reduction to the metallic state. Thus, the electrochemical process within these potential ranges can be described by two major reactions, respectively:

$$CuMo_6S_8 + 1.5Mg^{2+} + 3e^- \leftrightarrow CuMg_{1.5}Mo_6S_8 \quad (5)$$

$$CuMo_6S_8 + 2Mg^{2+} + 4e^- \leftrightarrow Mg_2Mo_6S_8 + Cu^0 \quad (6)$$

In these reactions we assumed that the oxidation state of Cu in the CPs is the same as that in $Cu_yMo_6T_8$, i.e. +1;[1,2] the formal charge of S is also constant, while Mg insertion is associated with respective change in the Mo oxidation state. Further, based on the classic thermodynamic approach (CV peaks are related to phase transitions) and the three redox peaks existing before Cu reduction, it is logical to divide the entire discharge process into four separate stages, where the fourth stage is the extrusion of copper:

$$CuMo_6S_8 + 0.5Mg^{2+} + e^- \leftrightarrow CuMg_{0.5}Mo_6S_8 \quad \text{(stoichiometric compound)} \quad (7)$$

$$CuMg_{0.5}Mo_6S_8 + 0.5Mg^{2+} + e^- \leftrightarrow CuMgMo_6S_8 \quad \text{(stoichiometric compound)} \quad (8)$$

$$CuMgMo_6S_8 + 0.5Mg^{2+} + e^- \leftrightarrow CuMg_{1.5}Mo_6S_8 \quad \text{(stoichiometric compound)} \quad (9)$$

$$CuMg_{1.5}Mo_6S_8 + 0.5Mg^{2+} + e^- \rightleftharpoons Mg_2Mo_6S_8 + Cu^0 \quad (10)$$

In the case that the electrochemical process is reversed before Cu extraction (Figure 3a), the three first stages are completely reversible and can be regarded formally as usual intercalation into pseudo-binary hosts. In the case of cycling over a wider range from 1.8 to 0.5 V (Figure 3b), the entire electrochemical process is also fully reversible because the curve shape does not change upon cycling. In spite of this overall chemical reversibility, the profile of the discharging curve below the baseline is completely different from that of the charging curve above the baseline. This may mean that the oxidation reactions differ from the reduction ones. In fact, partial electrode charge and subsequent electrochemical titration (insert, Figure 3b) shows that Cu metal can be oxidized to Cu^+ ions and reinserted back into the CPs' crystal structure. However, this insertion occurs in a few stages and can be completed only at significantly higher potentials.

As a first approximation, the total amount of charge involved in each of reactions (7)−(9) is assumed to be equal to one electron transfer. The reaction products are written

(37) Chevrel, R.; Sergent, M.; Prigent, J. *Mater. Res. Bull.* **1974**, *9*, 1487.
(38) McCusker, L. B.; Von Dreele, R. B.; Cox, D. E.; Louer, D.; Scardi, P. *J. Appl. Crystallogr.* **1999**, *32*, 36.

Table 1. Samples' Characterization (Results of the Rietveld Refinement of the Diffraction Profiles)

				lattice parameters					*R*-factors		
N	sample	intended composition	phase composition	a_h (Å)	c_h (Å)	V_h (Å^3)	relation to the el.-chem. curve	additional phases	χ^2	R_b	R_f
1	solid-state product	$Cu_{\sim 2}Mo_6S_8$	71% Phase III	9.570	10.259	814		1% MoS_2	0.55	3.80	2.40
			28% Phase II	9.521	10.314	810				5.41	2.68
2	leached product	$Cu_{\sim 1}Mo_6S_8$	65% Phase I	9.405	10.410	797	point 1	1% MoS_2	1.96	3.96	2.21
			34% Phase II	9.439	10.365	800				4.08	2.09
3	solid-state product	$Mg_{0.5}CuMo_6S_8$	74% $Mg_{0.1}Cu_{1.1}Mo_6S_8$	9.470	10.377	806	between points 1 and 2	4% Mo_2S_3 1% MoS_2	1.74	3.71	2.17
			21% $CuMo_6S_8$	9.420	10.401	799				3.95	2.33
4	solid-state product	$MgCuMo_6S_8$	42% $Mg_{0.1}Cu_{1.5}Mo_6S_8$	9.548	10.375	819	point 2	1% MgS 2% MoS_2	1.98	5.49	3.04
			37% $Mg_{0.7}Cu_{0.5}Mo_6S_8$	9.534	10.431	821				3.37	2.98
			19% $Mg_{0.4}Cu_{1.0}Mo_6S_8$	9.516	10.460	820				4.49	3.40
5	solid-state product	$Mg_{1.5}CuMo_6S_8$	97% $Mg_{0.8}Cu_{1.0}Mo_6S_8$	9.594	10.435	832	point 3	2% Mo 1% MgS	1.77	3.69	2.52
6	Electrode at 0.95 V	$Mg_{1.5}CuMo_6S_8$	34% $Mg_{1.8}Cu_{0.4}Mo_6S_8$	9.705	10.405	849	between points 3 and 4	0.5% MoS_2	1.78	3.71	2.94
			34% $Mg_{1.1}Cu_{1.6}Mo_6S_8$	9.724	10.392	851				4.67	3.13
			31.5% $Mg_{0.8}Cu_{1.0}Mo_6S_8$	9.594	10.435	832				11.2	3.90
7	electrode at 0.825 V	$Mg_{1.5}CuMo_6S_8$ + $Mg_2Mo_6S_8$ + Cu	47% $Mg_{0.1}Cu_{1.0}Mo_6S_8$	9.448	10.392	803	between points 4 and 5 + storage	0.2% MoS_2	0.49	5.58	2.72
			25% $CuMo_6S_8$	9.406	9.408	798				5.00	2.75
			22% $MgMo_6S_8$	9.477	10.531	819				4.65	3.08
			6% $Mg_2Mo_6S_8$	9.758	10.366	855				6.51	3.82
8	electrode at 0.5 V	$Mg_2Mo_6S_8$ + Cu	38% $Mg_{0.2}Cu_{0.9}Mo_6S_8$	9.462	10.434	809	point 5 + storage	1% Cu 1% MoS_2	0.80	5.40	3.00
			34% $MgMo_6S_8$	9.484	10.533	820				4.45	3.19
			14% $Mg_2Mo_6S_8$	9.761	10.369	856				5.19	3.50
			12% $CuMo_6S_8$	9.411	10.410	798				6.14	3.36
9	chem. intercalat.	$Mg_2Mo_6S_8$ + Cu	49% $MgMo_6S_8$	9.478	10.527	855	point 5 + storage	4.6% Cu 0.6% MoS_2	1.72	4.20	2.42
			40% $Mg_2Mo_6S_8$	9.759	10.369	819				4.60	2.54
			5% Mo_6S_8	9.201	10.878	797				5.60	2.85
10	chem. intercalat.*	$Mg_2Mo_6S_8$ + 2Cu	75% $Mg_2Mo_6S_8$	9.763	10.372	856		9% Cu 0.3% MoS_2	3.11	5.66	4.61
			15% $Mg_{0.5}Cu_{0.6}Mo_6S_8$	9.538	10.399	819				5.67	4.08
11	electrode at 1.36 V (charge)	$Mg_{0.6}Cu_{0.6}Mo_6S_8$ + Cu ?	40% Phase I of $CuMo_6S_8$	9.404	10.410	797	point 9 + storage	0.4% MoS_2	1.39	3.89	2.98
			59% Phase II of $CuMo_6S_8$	9.417	10.394	798				6.79	3.17

as stoichiometric compounds. However, as can be seen in Figure 3a, the intensities of the three CV peaks related to these reactions are not identical. It is difficult to determine the exact charge values because of the peaks' superposition, but the third reduction peak is obviously higher than the first two. As a result, we cannot be certain that reactions (7)−(9) reflect the reality. Moreover, the Li−Cu−Mo_6T_8 example[13−17] shows that the insertion process related to a system with two inserted species may differ fundamentally from the simple scenario proposed in the reaction scheme above, (7)−(9). Thus, a careful phase analysis of the intercalation products had to be carried out to verify the validity of these reactions.

Sample Characterization. Previous works[1,2,10,33,39] did not reveal any structural difference between the $M_xMo_6T_8$ (M = Cu, Li, or Mg) compounds obtained in three different ways: direct solid-state synthesis, electrochemical and chemical cation insertion. However, it was shown[10,39] that the Mg-containing CPs are extremely unstable outside the parent solution; thereby the phase composition is strongly effected by the environment under which the material is stored: The initial, pure phases obtained by electrochemical or chemical reactions can be detected only if the analysis is done rapidly after material preparation and the samples are contained in airtight holders. It was found[10,39] that $Mg_2Mo_6S_8$ oxidation during storage without visible oxygen access (only oxygen traces) is fundamentally similar to the electrochemical process upon charge of the battery because it results in successive formation of $MgMo_6S_8$ and Mo_6S_8 (see reactions (1) and (2)). The solid-state products exposed to air are stable, but only after formation of a compact, insulating MgO film on the material surface. As a result, the Mg content in these products is usually effectively smaller than that in the precursor mixture.[10,39]

Taking into account the materials' instability, we used for analysis not only the electrodes stopped at different points of the electrochemical curve (Figure 3) but also their analogs obtained by chemical and solid-state synthesis, to study Mg

(39) Levi, E.; Lancry, E.; Gofer, Y.; Aurbach, D. *Solid-State Electrochem.* **2006**, *10*, 176.

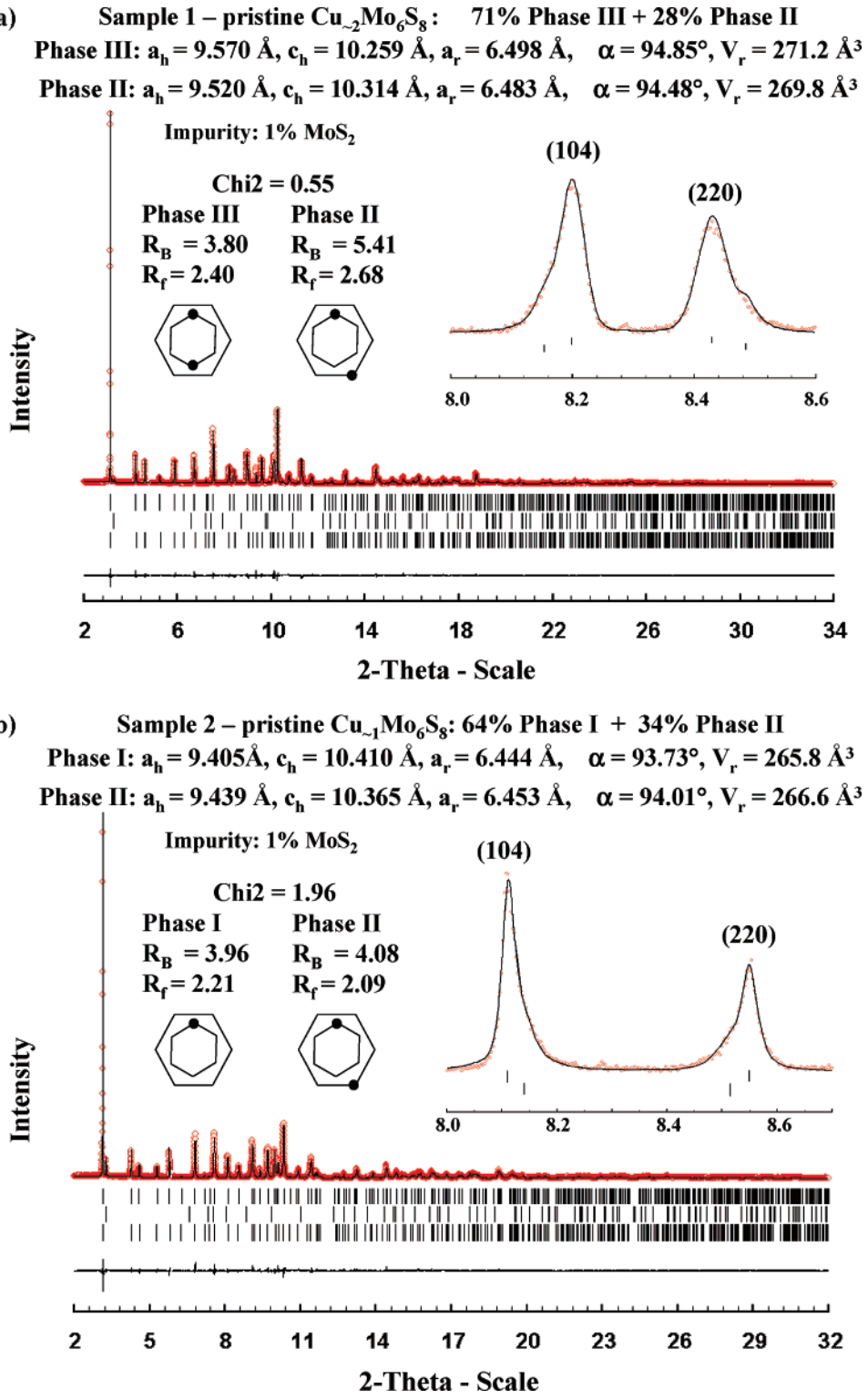

Figure 4. Synchrotron Rietveld profile for $Cu_yMo_6S_8$: (a) $y \approx 2$; (b) $y \approx 1$. The calculated 2θ values of the reflections (vertical bars) correspond to the major phases, MoS_2 and secondary phase (top-down).

insertion into $Cu_yMo_6S_8$ ($1 < y < 2$). Table 1 presents the intended and real compositions of the samples, the lattice parameters of the intercalation compounds, and their relation to the electrochemical curve. Phase analysis was done by the Rietveld method, and thereby, Table 1 includes also the data of the refinement quality (*R*-factors). As can be seen, in most of the experiments the products under study have a lower level of magnesiation than the intended one due to unavoidable Mg loss. Actually, the synchrotron measurements were performed for a higher number of the electrodes (points 2, 3, 7, 8), but the analysis showed their total demagnesiation; i.e., the electrodes' composition was similar to that of sample 11 ($Cu_{\sim 1}Mo_6S_8$).

As can be seen in Table 1, most of the samples under study are mixtures of different CPs with similar unit cell parameters. This leads to an extensive superposition of the

diffraction peaks related to these phases, as well as to a lower accuracy of their structural determinations. Thus, we also used the available electrochemical data (Figure 3) to verify the values of the cation occupancy obtained in the refinement.

Pristine $Cu_yMo_6S_8$ Phases ($1 \le y \le 2$). In spite of the intensive studies of the $Cu_yMo_6S_8$ compounds in the past, full structural characterization was made only for the metal-free host ($y = 0$) and for the products of the solid-state synthesis with $y \ge 1.8$.[1,2] The latter were found to be nonstoichiometric,[1,2,14,40−42] while for $0 < y < 1$ the electrochemical studies[40,41,43] showed a reaction of a classic phase transition:

$$Mo_6S_8 + Cu^+ + e^- \leftrightarrow CuMo_6S_8$$
(stoichiometric compound) (11)

The $1 < y < 2$ range seems to be the most intriguing. According to thermodynamic criteria, namely, the presence of a voltage plateau in the relevant chronopotentiometric curve (voltage vs time), this region should be related to a coexistence of two phases (or to reaction: $Cu^+ - e^+ + CuMo_6S_8 \rightarrow Cu_2Mo_6S_8$), but only one phase was found in previous studies.[40−43] Thus, the entire range of $y \ge 1$ (Cu_y-Mo_6S_8) was classified as a single phase, i.e., a solid solution. The unit cell parameters are well-established for $y = 1$ (JCPDS-ICDD, 34-1379: $a_h = 9.412(8)$ Å, $c_h = 10.407$-(10) Å, $V_h = 798$ Å^3) and for $y = 1.8$ ($a_h = 9.584$ Å, $c_h =$ 10.250 Å, $V_h = 815$ Å^3),[1,2] while within the range there is a substantial scattering of values presented by different researchers.[40−43] However, in general, it is clear that the increase of y in $Cu_yMo_6S_8$ results in the compression of the unit cell along the −3 symmetric axis, its expansion in the normal direction, and finally, in a higher unit cell volume.

As will be shown below, knowledge of the phase composition and the structure of pristine $Cu_yMo_6S_8$ compounds in the $1 < y < 2$ range is crucial for the understanding of the Mg insertion process. Hence, we performed the Rietveld analysis for the two intended compositions, Cu_2-Mo_6S_8 and $CuMo_6S_8$ (samples 1 and 2, or the products of the solid-state synthesis and the partial leaching, respectively, Figures 4a and 4b). As can be seen in the right-hand inserts in Figures 4a and 4b, the characteristic feature of Cu and Mg-containing CPs is the *hkl*-dependent asymmetry of the diffraction peaks. (Note that the peaks of the two samples with different *hkl* indexes differ by their asymmetry.) Commonly such asymmetry is caused by compositional gradient.[44] In our case it is related to a nonuniform Cu or Mg distribution in the CPs crystal structure. The latter may result from (i) environment instability of the phases (inhomogeneity in the same phase caused by Mg and Cu loss) and (ii) decomposition of solid solutions stable at higher temperature with formation of separate phases with close unit cell parameters.

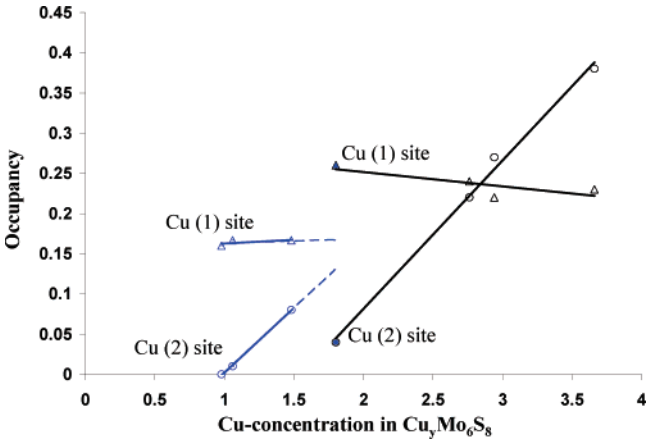

Figure 5. Site occupancy for the Cu (1) (inner ring) and the Cu (2) (outer ring) as a function of Cu concentration in the $Cu_yMo_6S_8$ compounds ($y \ge 1$) according to Yvon[1] (black color) and our data (blue color).

In the FULLPROF program, this asymmetry can be treated as an apparent strain[44] in the phase under study (a single-phase model) or as a mixture of a few phases, respectively. For the materials under study, the asymmetry was so pronounced that a satisfactory fitting was achieved only by using both the options. Thus, each of the samples 1 and 2 was presented in the Rietveld analysis as a mixture of two strained phases with different parameters (space group $R\bar{3}$). These two-phase models are in disagreement with the idea of a single solid solution for $y \ge 1$, which was presented in the previous publications.[40−43] It is clear that this new interpretation may have a real physical meaning only if these phases are structurally different.

To clarify the structural difference between these phases, we have to analyze the relation between cation distribution in the CPs and variations in the inner ring geometry with Cu content. Previously it was shown[1,2] that increase in y for $Cu_yMo_6S_8$ ($y \ge 1.8$) results in a higher Cu presence in the outer ring, while the occupancy of the inner ring remains almost constant and equal to 0.22−0.26 (black lines in Figure 5), i.e., the inner ring can adopt up to two Cu^+ cations. (The occupancy of 1/6 corresponds to one cation per formula unit.) Based on these structural data, one can assume that, in the range of $1 < y < 1.8$, the $Cu_yMo_6S_8$ compound should have a similar cation distribution; i.e., mainly the inner sites should be occupied. Thus, Cu insertion in this range should result in a change in the occupancy in the inner ring from 1/6 to 0.26.

However, simple geometric considerations show that such a structural model is not reasonable. First, the distribution of the two cations in the inner ring in $Cu_yMo_6S_8$ ($y \ge 1.8$) cannot be independent: Because of the short distances between the sites, the only possible arrangement for the two cations is the simultaneous occupancy of the opposite sites within the ring or the formation of Cu−Cu pairs. (Note that the rhombohedral symmetry is not really in disagreement with the existence of such pairs, but presumes their random orientation throughout the CPs' crystal structure.) Even in this case, the distance between these two cations in $Cu_{1.8}$-Mo_6S_8 is rather small (2.52 Å), which is evidence of metallic

(40) Schollhorn, R.; Kumpers, M.; Lerf. A.; Umlauf, E.; Schmidt, W. *Mater. Res. Bull.* **1979**, *14*, 1039.
(41) Fischer, C.; Gocke, E.; Stege, U.; Schollhorn, R. *J. Solid State Chem.* **1993**, *102*, 54.
(42) Flukiger, R.; Baillif, R.; Muller, J.; Yvon, K. *J. Less Common Met.* **1980**, *72*, 193.
(43) Tovar, M.; DeLong, L. E.; Jonston, D. C.; Maple, M. B. *Solid State Commun.* **1979**, *30*, 551.
(44) Delhez, R.; de Keijser, T. H.; Langford, J. I.; Louer, D.; Mittemeijer, E. J.; Sonneveld, E. J. In *The Rietveld Method*; Young, R. A., Ed.; IUCr, Oxford University Press: Oxford, 1993.

Table 2. Cation−Cation Distances

(a) In Pristine $Cu_yMo_6S_8$

N	intended composition	phase, lattice parameters (Å)	Mo−Mo (Å)	VEC	Mo−M1 (Å)	Mo−M2 (Å)	M1−M1 (Å)	M2−M1 (Å)	M2−M2 (Å)
1	$Cu_{\sim 2}Mo_6S_8$	III $a_h = 9.570$ $c_h = 10.259$	2 × 2.686(2) 2 × 2.756(2) 3.227(2)	3.63	3.18(1)	2.99(3) 3.03(3) 3.09(3)	2 × 1.28(1) 2 × 2.17(1) 2.520(2)	1.39(3) 2.00(3) 2.49(3) 2.94(3) 3.07(3) 3.29(3)	1.85(4) 2 × 3.11(4) 2 × 3.69(4)
		II $a_h = 9.520$ $c_h = 10.314$	2 × 2.692(3) 2 × 2.763(3) 3.189(2)	3.57	3.46(3)	3.02(3) 3.12(3) 3.14(3)	2 × 0.91(5) 2 × 1.58(3) 1.82(2)	1.47(3) 1.62(3) 2.22(4) 2.40(4) 2.84(3) 2.92(3)	2.47(4) 2 × 2.73(4) 2 × 3.27(4)
2	$Cu_{\sim 1}Mo_6S_8$	I $a_h = 9.405$ $c_h = 10.410$	2 × 2.704(2) 2 × 2.792(2) 3.135(2)	3.50	3.48(2)	-	2 × 0.82(3) 2 × 1.42(2) 1.64(1)		
		II $a_h = 9.439$ $c_h = 10.365$	2 × 2.694(3) 2 × 2.774(3) 3.146(2)	3.51	3.48(3)	2.98(3) 3.02(3) 3.02(3)	2 × 0.84(4) 2 × 1.45(3) 1.68(2)	1.84(4) 1.99(4) 2.49(4) 2.70(4) 3.08(4) 3.17(3)	1.73(4) 2 × 3.25(4) 2 × 3.68(5)

(b) In Mixed CPs

N	CP	Mo−Mo (Å)	VEC	Mo−M1 (Å)	Mo−M2 (Å)	M1−M1 (Å)	M2−M1 (Å)	M2−M2 (Å)
6	$Mg_{0.7}Cu_{0.5}Mo_6S_8$ $a_h = 9.534$ $c_h = 10.431$	2 × 2.684(4) 2 × 2.729(4) 3.265(3)	3.65	3.40(2)	3.04(3) 3.04(3) 3.09(2)	2 × 0.98(3) 2 × 1.70(3) 1.96(2)	1.72(3) 2.01(3) 2.47(3) 2.81(3) 3.16(3) 3.29(3)	1.74(3) 2 × 3.25(4) 2 × 3.69(3)
7	$Mg_{0.8}CuMo_6S_8$ $a_h = 9.594$ $c_h = 10.435$	2 × 2.671(1) 2 × 2.711(1) 3.286(1)	3.75	3.36(2)	3.06(1) 3.09(1) 3.11(1)	2 × 1.07(2) 2 × 1.86(2) 2.15(1)	1.58(1) 1.88(2) 2.45(2) 2.76(2) 3.18(2) 3.34(1)	1.99(1) 2 × 3.09(1) 2 × 3.62(1)
8	$Mg_{1.1}Cu_{1.6}Mo_6S_8$ $a_h = 9.724$ $c_h = 10.392$	2 × 2.653(4) 2 × 2.679(3) 3.379(3)	3.96	3.40(3)	3.02(1) 3.15(1) 3.17(1)	2 × 1.12(3) 2 × 1.93(3) 2.23(2)	1.66(2) 2.06(2) 2.52(2) 2.95(2) 3.21(2) 3.29(2)	1.76(1) 2 × 3.33(1) 2 × 3.75(1)
9	$Mg_{1.8}Cu_{0.4}Mo_6S_8$ $a_h = 9.705$ $c_h = 10.405$	2 × 2.661(4) 2 × 2.666(5) 3.354(5)	4.00	3.35(3)	3.05(1) 3.10(1) 3.18(1)	2 × 1.16(4) 2 × 2.00(3) 2.31(2)	1.74(2) 2.08(3) 2.60(3) 3.04(3) 3.13(2) 3.42(2)	1.58(2) 2 × 3.41(2) 2 × 3.88(2)

interactions in the pairs. Compounds with a lower Cu amount should have smaller inner ring dimensions because the ring radius (so-called cation delocalization in CPs) correlates with the unit cell parameters.[1,2]

According to our refinement (Table 2a), the longest distance between the cation sites in the inner ring of $CuMo_6S_8$ is equal to 1.64 Å. This value is confirmed by a similar distance in $CuMo_6Se_8$, which is equal to 1.76 Å. (It is known[1,2] for other CPs that the sulfide and selenide analogs of the same cation have similar delocalization values.) It is clear that such a distance is too short for the formation of the Cu−Cu pairs. Moreover, we believe that $y = 1.8$ is the minimal Cu amount that allows for the formation of the Cu−Cu pairs in the inner ring. Below this critical value the occupancy of the ring should be equal to 1/6 (one cation per ring), while all additional cations should be located in the outer rings. Thus, the following three phases should exist in the $1 \leq y \leq 1.8$ range:

1. Phase I: stoichiometric $CuMo_6S_8$ ($y = 1$) with a single Cu^+ cation (per formula unit) in the inner ring.

2. Phase II: nonstoichiometric $Cu_yMo_6S_8$ ($1 < y < 1.8$) with a single Cu^+ cation in the inner ring and various amounts ($y - 1 < 0.8$) of Cu^+ cations in the outer sites.

3. Phase III: well-known $Cu_{1.8}Mo_6S_8$ with a preferential occupancy of the inner sites.[1,2]

This structural concept correlates well with the two-phase interpretation used in the refinement procedure. The models of the main phases for the $Cu_{\sim 1}Mo_6S_8$ and $Cu_{\sim 2}Mo_6S_8$

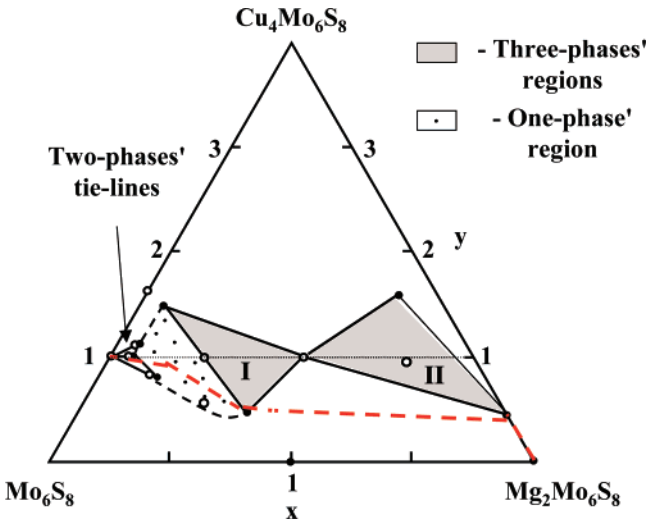

Figure 6. Proposed phase diagram of Mg insertion into $Cu_{\sim 1}Mo_6S_8$. The open and solid circles present the composition of the samples and the intercalation compounds, respectively. The black and red dotted lines follow the variation of the electrode composition during Mg insertion and extraction, respectively.

materials correspond to Phases I and III, respectively, while the secondary phases in both materials can be regarded as the same Phase II or solid solution with different amount of Cu. As can be seen in Figure 4, for $Cu_{\sim 2}Mo_6S_8$, the dimensions of the unit cell for the main component are very close to that of $Cu_{1.8}Mo_6S_8$, but 29% of the material has a smaller unit cell due to the lower Cu concentration. For $Cu_{\sim 1}Mo_6S_8$, the main component is very close to the standard one (JCPDS-ICDD, 34-1379), but 34% of the material has a higher Cu content. The differences in the cation distribution for two phases in each material are shown in the left inserts of Figure 4. Based on the results of the refinement, we can supplement the site occupancy in the rings vs y in $Cu_yMo_6S_8$ compounds found previously for $y \geq 1.8$ (the black lines in Figure 5)[1,2] with the data for $1 \geq y < 1.8$ (the blue lines in Figure 5).

Interestingly, Phase II is presented in both of the samples as an additional phase, while the diffraction peaks of this phase are much broader than those of the main phases. The structural distortion of Phase II may result from the lower air stability of this phase. The latter can explain the spreading of the experimental data achieved in different environments: the unit cell parameters measured under air should be related mainly to more stable Phases I and III, while the in situ experiments should demonstrate mostly the continuous changes in Phase II. Such a complex phase composition agrees well with the presence of the potential plateau in the electrochemical curve associated with this range.[40,41,43] In addition, the analysis of sample 1 (i.e., the pristine material, see Figures 3a and 3b and Table 1) shows that similar to the compounds synthesized by the solid-state method ($y \geq 1.8$), it is difficult to obtain a single-phase $Cu_yMo_6S_8$ host with the exact stoichiometry of $y = 1$ by leaching.

Phase Diagram of Mg Insertion into $CuMo_6S_8$. Figure 6 shows the part of the ternary phase diagram studied in this work and relates to Mg insertion into the $CuMo_6S_8$ host (the black dotted line follows the variation of the electrode composition during this process). In the first stage, the insertion of magnesium results in the formation of the $Mg_{0.1}CuMo_6S_8$ phase. The reaction proceeds as a phase transition, which is evidenced by the fact that in sample 7 (Figure 3, Table 1) the latter compound coexists with $CuMo_6S_8$. A similar coexistence was found for samples 3 and 8 (Figure 3, Table 1), but the Mg/Cu ratio in the mixed phases was slightly different.

Based on the presence of compounds such as $Mg_{0.4}CuMo_6S_8$ and $Mg_{0.5}Cu_{0.6}Mo_6S_8$ in samples 4 and 10, respectively (Figure 3, Table 1), we marked out the single-phase region in Figure 6. Thus, the formation of solid solutions, $Mg_xCuMo_6S_8$ ($0.1 < x < 0.4$), is suggested for the second intercalation stage. However, additional studies are needed to verify this suggestion. These two stages cannot be seen separately in the electrochemical curves (Figure 3), both of which appear as a singe CV peak between points 1 and 2 in Figure 3a. The final stoichiometry of the process, $x = 0.4$, agrees well with the specific capacity (about 0.8 electrons per formula) related to this peak.

At the $x = 0.4$ point (sample 4), the solid solution decomposes into two new phases, $Mg_{0.1}Cu_{1.5}Mo_6S_8$ and $Mg_{0.7}Cu_{0.5}Mo_6S_8$. A typical feature of this decomposition is the cation segregation, similar to that found for the Li−Cu−Mo_6S_8 system.[14] It can be suggested that further Mg insertion (region I, Figure 6) is associated with the coexistence of three phases: those mentioned above and $Mg_{0.8}CuMo_6S_8$ (sample 5). The stoichiometry of the latter compound is in accordance with the specific capacity (about 0.8 electrons) related to the second CV peak between points 2 and 3 in Figure 3a.

The data for sample 6 (Table 1) seem to prove the presence of the second three-phase region in the phase diagram, where $Mg_{0.8}CuMo_6S_8$ coexists with $Mg_{1.1}Cu_{1.6}Mo_6S_8$ and $Mg_{1.8}Cu_{0.4}Mo_6S_8$. According to the composition of these three phases, it is clear that, after the formation of the compound with a uniform cation distribution for $x = 0.8$, cation segregation occurs again for higher x. The phase transitions, which take place in this region, results in a third CV peak between points 3 and 4 in Figure 3a. As the tie line between $Mg_{1.1}Cu_{1.6}Mo_6S_8$ and $Mg_{1.8}Cu_{0.4}Mo_6S_8$ does not follow the phase diagram boundary (Figure 6), some additional process of phase transitions should proceed in the system before it reaches the exact $Mg_{1.5}CuMo_6S_8$ stoichiometry (the highest intercalation level of Mg before Cu extrusion). However, this process does not appear as a separate CV peak.

Thus, instead of reactions (7)−(9), suggested above as a starting point, the real process of reversible Mg intercalation into $CuMo_6S_8$ before Cu extrusion can be presented by the following three major stages:

$$CuMo_6S_8 + 0.4Mg^{2+} + 0.8e^- \leftrightarrow CuMg_{0.4}Mo_6S_8 \quad (7')$$

$$CuMg_{0.4}Mo_6S_8 + 0.4Mg^{2+} + 0.8e^- \leftrightarrow CuMg_{0.8}Mo_6S_8 \quad (8')$$

$$CuMg_{0.8}Mo_6S_8 + 0.7Mg^{2+} + 1.4e^- \leftrightarrow CuMg_{1.5}Mo_6S_8 \quad (9')$$

In accordance with reaction (10), further Mg insertion results in Cu extraction. Short XRD experiments performed for fresh, fully intercalated products show the mixture of $Mg_2Mo_6S_8$ and metallic Cu. However, the phase composition

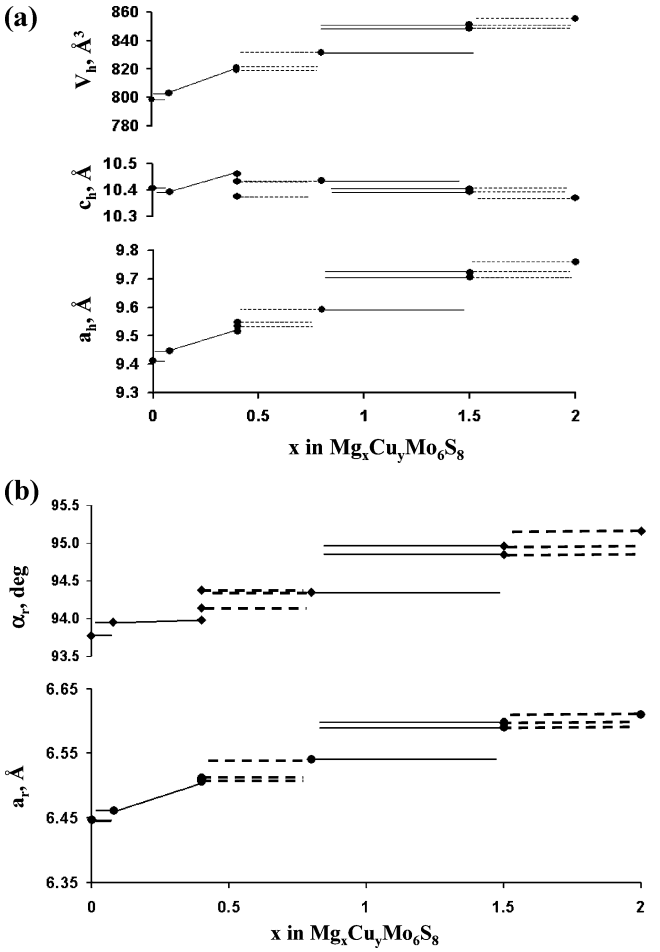

Figure 7. Change in the dimensions of the hexagonal and the rhombohedral unit cells of the intercalation compounds upon Mg insertion into $Cu_{\sim 1}Mo_6S_8$.

of the same samples after their storage may be essentially different (Table 1). Products obtained by chemical Mg intercalation and stored under air (samples 9 and 10) contain relatively high amounts of $Mg_2Mo_6S_8$ and metallic Cu. In contrast, in the electrodes stored without visible oxygen access (samples 7 and 8), the metallic Cu remains active and returns to the CP crystal structure upon material oxidation, forming mixed Cu−Mg phases and $CuMo_6S_8$. The presence of the latter compound in almost all the electrodes under study confirms the total reversibility of the entire electrochemical process (reaction (6)).

Figure 7 shows the variations in the unit cell dimensions for the Mg−Cu−Mo_6S_8 system. Mg insertion results mostly in higher a_h, a_r, α_r, and V_h values, while the changes in the c_h parameter are relatively small; i.e., the expansion of the CPs' framework occurs in directions normal to the −3 symmetric axis. This result is in agreement with the lattice parameters of the ternary compounds, $CuMo_6S_8$ and $Mg_2Mo_6S_8$, which differ mainly by a_h values (Table 1).

Thus, in spite of some unclear details of the phase diagram caused by its complex character, the correlation between the electrochemical reactions and variations in the phase composition upon Mg insertion was successfully established.

Crystal Structure of the Mixed Mg−Cu−Mo_6S_8 Compounds and the Mg Insertion Mechanism. Figure 8 shows the cation distribution in the mixed intercalation compounds.

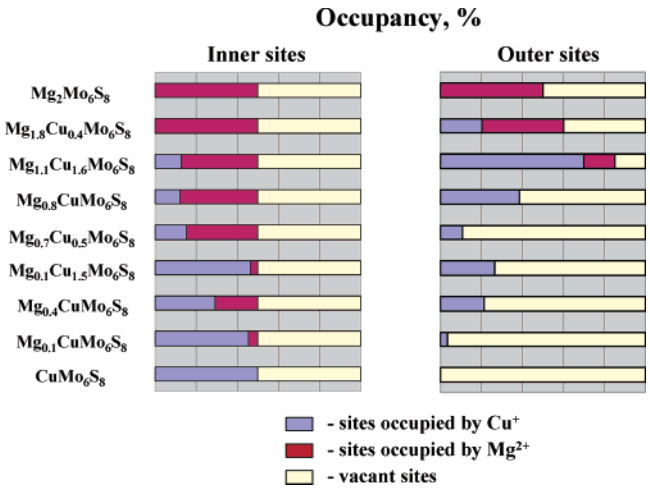

Figure 8. Cation distribution in the mixed intercalation compounds.

The latter can be defined as nonstoichiometric phases, $Mg_xCu_yMo_6S_8$. In general, Mg insertion results in a decrease of Cu in the inner sites and its respective increase at the outer sites. It means that the inserting Mg^{2+} cations push out the Cu^+ ions from the inner to the outer sites. This Mg preference for the inner sites can be explained by a stronger repulsion between Mo atoms and divalent Mg^{2+} cations, as compared to that between Mo and monovalent Cu^+ ions. In fact, the distances between Mo and the inner sites are essentially longer than those between Mo and the outer sites (compare the Mo−M1 and Mo−M2 distances in Table 2b). However, the correlation between the Cu content in the outer sites and the intercalation level is not direct. It appears only as a general tendency because of the cation segregation mentioned above. In addition, it can be seen that a total, Cu and Mg, occupancy of the inner ring for all the phases is only one cation per ring because the maximal distance in the inner ring of these compounds (M1−M1 in Table 2b) is too small to allow for the presence of two cations.

Based on the data of Figure 8 and Table 2b, we can propose a comprehensive structural mechanism for Mg insertion into $CuMo_6S_8$. Figure 9 presents different cation assemblies in the inner and outer rings, as well as their relative amount in the crystal structure of the intercalation compounds. According to these structural fragments, all mixed phases can be divided into three groups. The compounds of the first group have the same three fragments with (i) single Cu, (ii) single Mg, and (iii) two Cu atoms, while the concentration of the two latter fragments increases for a higher intercalation level. Thus, we believe that, at the earlier stages of Mg insertion, the Cu atom, which is pushed by Mg from its inner site, prefers to leave the parent group of the cation sites and to form the assembly with other Cu^+ cations, to ensure a more uniform distribution of the cation charge in the structure: two electrons for the Cu^+−Cu^+ assembly instead of three electrons for the Cu^+−Mg^{2+} one. As a result, the total charge in different cation groups for this intercalation level varies from one to two electrons.

Initially, this process appears as cation segregation within the same crystal structure: As a result of the coordinated Mg and Cu rearrangement, the number of fragments with a

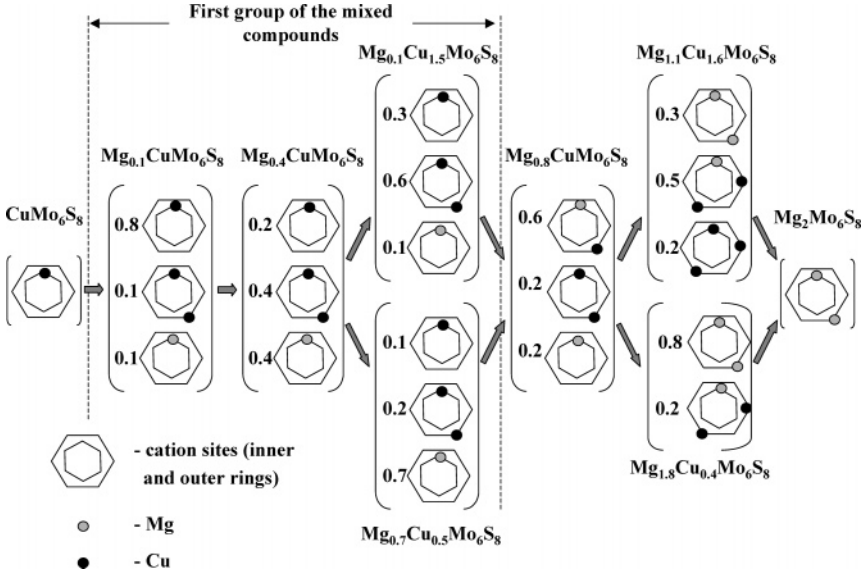

Figure 9. Proposed structural mechanism of Mg insertion into $Cu_{\sim 1}Mo_6S_8$. The cation distribution within the rings is shown in the form of the structural fragments (in brackets) typical for the given compound. The numbers are the contents of the fragments.

single Mg atom is equal to that with two Cu atoms. However, their ratio changes drastically after cation segregation in separate phases (for $x = 0.4$): The fragments with a single Mg^{2+} cation are prevalent in $Mg_{0.7}Cu_{0.5}Mo_6S_8$, while $Mg_{0.1}Cu_{1.5}Mo_6S_8$ is comprised mostly of the Cu-containing fragments. In spite of this variation, all the phases of the first group should form the same solid solution at higher temperature, which decomposes at ambient conditions.

A first mixed Mg−Cu assembly appears in $Mg_{0.8}CuMo_6S_8$, where the total charge in the different cation groups varies from two to three electrons. In the mixed compounds with the highest intercalation level (the two last compounds in Figure 9, before Cu extraction) we can see three new assemblies, which include (i) three Cu^+ cations, (ii) two Mg^{2+} cations, and (iii) one Mg^{2+} plus two Cu^+ cations. Because of the cation segregation, Cu-rich $Mg_{1.1}Cu_{1.6}Mo_6S_8$ contains all the assemblies, while Cu-depleted $Mg_{1.8}Cu_{0.4}Mo_6S_8$ has only two of them, and its composition is close to the final intercalation product, $Mg_2Mo_6S_8$. The total charge in the separate cation groups varies from three to four electrons.

Thus, in general, the crystal structure of the quaternary intercalation compounds in the Mg−Cu−Mo_6S_8 system is really similar to that of the ternary phases: both Mg^{2+} and Cu^+ cations are located in the tetrahedral sites of the inner and outer rings, and their occupancy depends on the intercalation level. However, the cation distribution is not disordered. It can be characterized by (i) Mg preference for the inner sites and (ii) cation segregation. The latter is typical for the separate cation groups in the same intercalation compound (Cu−Cu assemblies), but it can appear also as cation segregation in different phases (mixtures of Cu-rich and Cu-depleted CPs).

Structural Mechanism of Mg Deinsertion from Cu−$Mg_2Mo_6S_8$. The red line in Figure 6 shows the change in the electrode composition upon Mg deinsertion. According to the values of the specific capacity related to the separate CV peaks in Figure 3b and the data of the Cu titration (insert in Figure 3b), this process can be presented by the following reactions:

$$Mg_2Mo_6S_8 + 0.4Cu^0 - 0.4e^- \leftrightarrow Mg_{1.8}Cu_{0.4}Mo_6S_8 + 0.2Mg^{2+} \quad (12)$$

$$Mg_{1.8}Cu_{0.4}Mo_6S_8 + 0.1Cu^0 - 2e^- \Rightarrow Mg_{0.8}Cu_{0.5}Mo_6S_8 + Mg^{2+} \quad (13)$$

$$Mg_{0.8}Cu_{0.5}Mo_6S_8 + 0.1Cu^0 - 0.4e^- \Rightarrow Mg_{0.6}Cu_{0.6}Mo_6S_8 + 0.2Mg^{2+} \quad (14)$$

$$Mg_{0.6}Cu_{0.6}Mo_6S_8 + 0.3Cu^0 - 0.6e^- \Rightarrow Mg_{0.3}Cu_{0.9}Mo_6S_8 + 0.3Mg^{2+} \quad (15)$$

$$Mg_{0.3}Cu_{0.9}Mo_6S_8 + 0.1Cu^0 - 0.6e^- \Rightarrow CuMo_6S_8 + 0.3Mg^{2+} \quad (16)$$

According to its chemical composition, the product of reaction (12), corresponding to point 7 in Figure 3a should be identical to the last Cu-depleted phase, $Mg_{1.8}Cu_{0.4}Mo_6S_8$. Thus, the first anodic peak in the CV of Figure 3b (around 1 V) can be described as a Cu ⇔ Mg exchange. Concerning the other products of the Mg deinsertion process, except for the final formation of $CuMo_6S_8$, we cannot be sure that they have the exact analogs, as described above, during the course of Mg insertion. These products may also be a mixture of some phases. In spite of this uncertainty in the phase composition, we can use reactions (12)−(16) and the structural changes established for Mg insertion into $CuMo_6S_8$ (Figure 9) to propose a general mechanism for Mg deinsertion as well (Figure 10). The latter is based on the speculation that the intercalation compounds formed upon Mg insertion and deinsertion into $CuMo_6S_8$, in spite of their stoichiometric difference, should include the same structural fragments that depend only on the intercalation level.

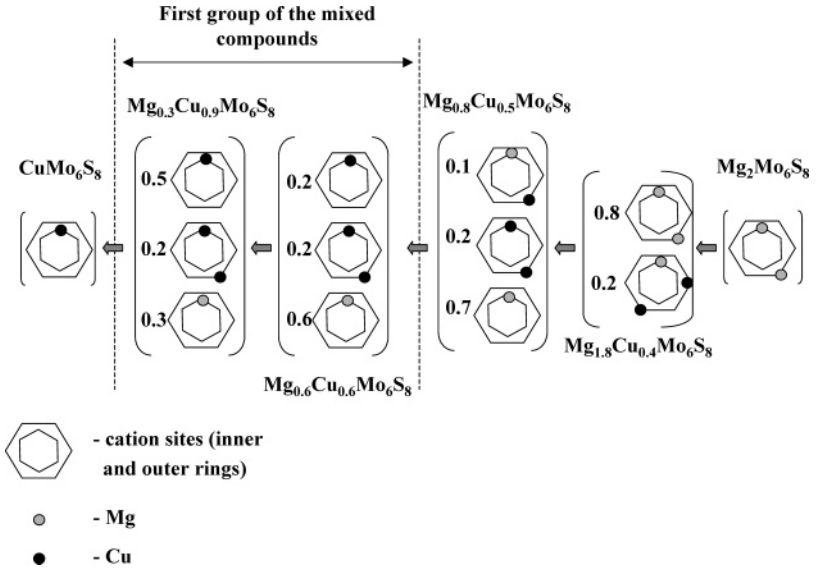

Figure 10. Proposed structural mechanism of Mg deinsertion and Cu insertion in the Cu−Mg−Mo_6S_8 system.

According to the proposed structural mechanism (Figure 10), reaction (13), or the second anodic CV peak with a high intensity (Figure 3a), is related mainly to Mg removal from the outer sites of the crystal structure, while the Cu ⇔ Mg exchange during this process is relatively small. The structural fragments in the product of this reaction should be identical to those proposed for $Mg_{0.8}CuMo_6S_8$. The last three anodic CV peaks between points 8 and 11 in Figure 3b are associated with subsequent substitution of Mg in the inner sites by Cu^+ cations. Thus, the products of reactions (14) and (15) should be related to the first group's compounds, discussed above for the Mg insertion. As expected, Cu ⇔ Mg substitution prevents the Mg trapping that is typical for the Mo_6S_8 host at room temperature. In fact, Cu^+ cations inserting upon the anodic (charging) process push the Mg^{2+} ions from their inner sites with low potential energy to the outer sites. As a result, the Mg^{2+} cations can move freely throughout the material bulk.

Conclusions

A combination of cyclic voltammetry and ex situ high-resolution synchrotron X-ray diffraction was used to study the phase diagram of Mg insertion into $Cu_{\sim 1}Mo_6S_8$. The host, $Cu_yMo_6S_8$ ($1 \le y \le 1.8$), was presented by three phases with different cation distributions: (i) a single Cu^+ cation (per formula unit) in the inner ring (stoichiometric phase I for $y = 1$), (ii) a single Cu^+ cation in the inner ring and various amounts of Cu^+ cations in the outer sites (nonstoichiometric Phase II for $1 < y < 1.8$), and (iii) the well-known $Cu_{1.8}Mo_6S_8$, compound in which the inner sites can be occupied by two Cu^+ cations (nonstoichiometric Phase III).

By the Rietveld analysis for nine new $Mg_xCu_yMo_6S_8$ phases, it was shown that the crystal structure of the quaternary intercalation compounds in the Mg−Cu−Mo_6S_8 system is similar to that of the ternary phases: both Mg^{2+} and Cu^+ cations are located in the tetrahedral sites of the inner and outer rings, while the occupancy of the sites increases with intercalation level. However, the cation distribution is not disordered, and it can be characterized by (i) Mg-ion preference for the inner sites and (ii) cation segregation. The latter is typical for the separate cation groups in the same intercalation compound (Cu−Cu assemblies), but it appears also as cation segregation in different phases. As a result, similar to the known Li−Cu−Mo_6S_8 system, the phase diagram of Mg insertion into $Cu_{\sim 1}Mo_6S_8$ is complex. It includes three phase regions and the coexistence of Cu-rich and Cu-depleted compounds. The proposed structural mechanism of Mg intercalation was used to explain the peculiarities of the electrochemical behavior of the $Cu_{\sim 1}Mo_6S_8$ host, in particular, the absence of the Mg trapping phenomenon typical for the metal-free Mo_6S_8 host.

Acknowledgment. Partial support for this work was obtained from the Israel-US Binational Foundation (BSF). We acknowledge the European Synchrotron Radiation Facility for the provision of synchrotron radiation facilities and we would like to thank Prof. A. Fitch for assistance in using the beamline.

Supporting Information Available: Crystallographic information (CIF) for the following compounds: (1) $Cu_{1.0}Mo_6S_8$; (2) $Cu_{1.4}Mo_6S_8$; (3) $Mg_{0.1}Cu_{1.1}Mo_6S_8$; (4) $Mg_{0.1}Cu_{1.5}Mo_6S_8$; (5) $Mg_{0.7}Cu_{0.5}Mo_6S_8$; (6) $Mg_{0.4}Cu_{1.0}Mo_6S_8$; (7) $Mg_{0.8}Cu_{1.0}Mo_6S_8$; (8) $Mg_{1.1}Cu_{1.6}Mo_6S_8$; (9) $Mg_{1.8}Cu_{0.4}Mo_6S_8$; (10) $Mg_{0.1}Cu_{1.0}Mo_6S_8$; (11) $Mg_{0.2}Cu_{0.9}Mo_6S_8$. Rietveld profiles for all the samples under study. Structural parameters of pristine materials and mixed CPs in the form of a table. This material is available free of charge via the Internet at http://pubs.acs.org.

CM0715489